Publications of the Astronomical Society of the Pacific, 134:044201 (16pp), 2022 April https://doi.org/10.1088/1538-3873/ac6195

A Deep Investigation of Two Poorly Studied Open Clusters Haffner 22 and Melotte 71 in the Gaia era

D. Bisht[1], Qingfeng Zhu[1], R. K. S. Yadav[2], Geeta Rangwal[3], Devesh P. Sariya[4], Alok Durgapal[5], and Ing-Guey Jiang[4]
[1] Key Laboratory for Researches in Galaxies and Cosmology, University of Science and Technology of China, Chinese Academy of Sciences, Hefei, Anhui, 230026, People's Republic of China; dbisht@ustc.edu.cn
[2] Aryabhatta Research Institute of Observational Sciences, Manora Peak, Nainital 263129, India
[3] Indian Institute of Astrophysics, Koramangala II BLock, Bangalore, 560034, India
[4] Department of Physics and Institute of Astronomy, National Tsing-Hua University, Hsin-Chu, Taiwan
[5] Center of Advanced Study, Department of physics, D.S.B. campus, Kumaun University, Nainital, 263002, India
Received 2021 October 21; accepted 2022 March 28; published 2022 April 26

Abstract

This paper presents a deep investigation of two open clusters, Haffner 22 and Melotte 71, using astrometric and photometric data from Gaia EDR3. We identified 382 and 597 most probable cluster members with membership probability higher than 50%. Mean proper motions in R.A. and decl. are estimated as $(-1.631 \pm 0.009, 2.889 \pm 0.008)$ and $(-2.398 \pm 0.004, 4.210 \pm 0.005)$ mas yr^{-1} for Haffner 22 and Melotte 71, respectively. A comparison of observed CMDs with the theoretical isochrones leads to an age of 2.25 ± 0.25 and 1.27 ± 0.14 Gyr for these clusters. The distances 2.88 ± 0.10 and 2.28 ± 0.15 kpc based on the parallax are comparable with the values derived by the isochrone fitting method. Five and four blue straggler stars (BSS) are identified as cluster members in Haffner 22 and Melotte 71. Based on the relative number of high-velocity (binary) and single stars, we inferred binary fractions for both clusters in the range of $\sim 10\% \leqslant f_{\rm bin} \leqslant 14\%$, for both core and o?-core regions. We found binary content is larger in the core region. Mass function slope is in good agreement with the Salpeter's value for Melotte 71 ($x = 1.23 \pm 0.38$ within mass range 1–3.4 $M_{\odot}$) while it is quite a flat slope for Haffner 22 ($x = 0.63 \pm 0.30$ within mass range 1–2.3 $M_{\odot}$). Evidence for the existence of mass-segregation effect is observed in both clusters. Using the Galactic potential model, Galactic orbits are derived, indicating that both clusters follow a circular path around the Galactic center, evolving slowly.

Unified Astronomy Thesaurus concepts: Open star clusters (1160); Binary stars (154); Initial mass function (796); Stellar dynamics (1596); Blue straggler stars (168)

1. Introduction

Open clusters (OCs) in the Milky Way span a wide range in ages, distances, and chemical compositions (Dias et al. 2002; Kharchenko et al. 2013; Cantat-Gaudin et al. 2020). The (early) Third Gaia Data Release 3 (hereafter EDR3; Gaia Collaboration et al. 2021) of Gaia mission was made public on 2020 December 3rd. This data contains the central coordinates, proper motions in both the R.A. and decl. and parallax (α, δ, $\mu_{\alpha}\cos\delta$, μ_{δ}, π) for more than 1.4 billion sources within the limit of 3 to 21 mag in G band. We can provide an estimation of cluster membership to enhance our understanding of the fundamental parameters of OCs. Cantat-Gaudin et al. (2018) provided a membership probability catalog for 1229 OCs using Gaia DR2 for stars up to 18 mag in the G band. Recently they added few more clusters to get a catalog of 1481 OCs (Cantat-Gaudin & Anders 2020). Liu & Pang (2019) used the Friend of Friend (FoF) method to find 2443 OCs and select their probable members. The FoF method is based on the galaxy group finder algorithm proposed by Yang et al. (2005). Sim et al. (2019) listed 655 cluster candidates (207 new candidates) based on the visual inspection of the stellar distributions in proper motion space and spatial distributions in the Galactic coordinates space. Monteiro et al. (2020) investigated 45 OCs using the maximum likelihood method to estimate membership in cluster regions. Ferreira et al. (2020) discovered 25 new OCs and identified probable members using a decontamination procedure to the three-dimensional astrometric space.

Both clusters are very sparse and located in the third Galactic quadrant. They are situated very near to the Galactic disk hence highly contaminated by field stars. Very few studies are available for these clusters. Haffner 22 and Melotte 71 fields of view contain a large number of field stars so it is very necessary to separate those stars from the actual cluster stars to identify accurate fundamental parameters. Mass function and

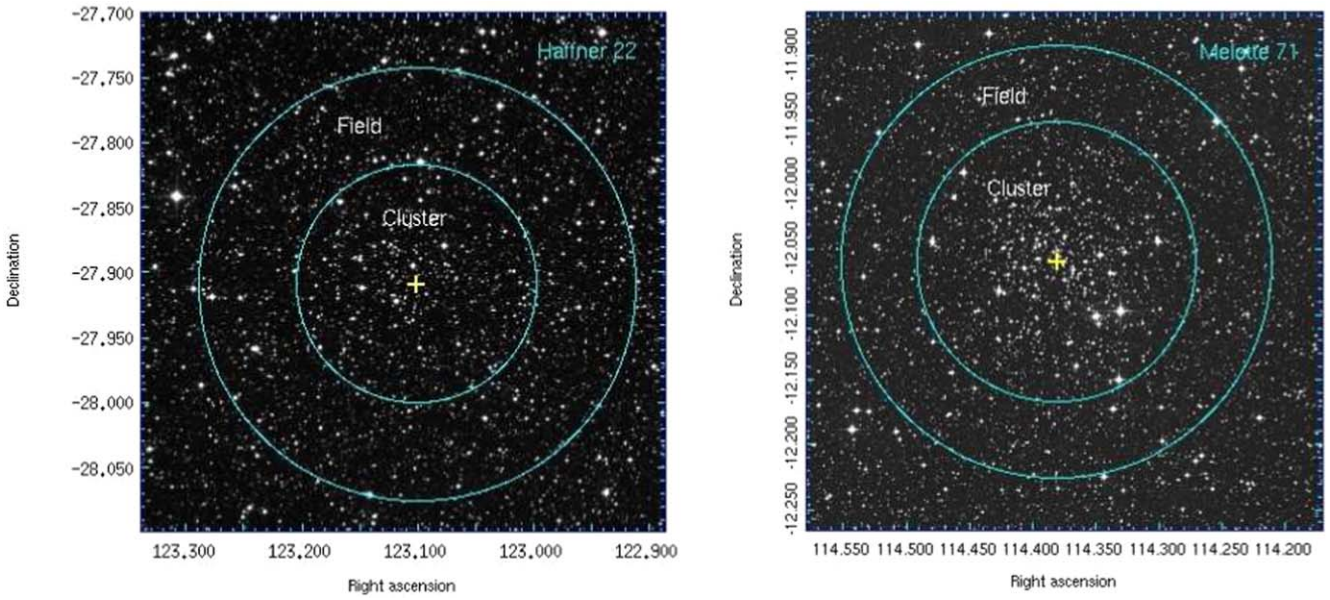

Figure 1. Identification maps of clusters Haffner 22 and Melotte 71 taken from the Leicester Database and Archive Service. The inner-circle indicates the radius of clusters, while the outer circle indicates the radius of data extraction in this study. Plus sign indicates the cluster center.

segregation are not well known for Haffner 22, while for Melotte 71, it has been done without selecting cluster members. The Gaia EDR3 data enable us to distinguish cluster members and study the structural properties and the dynamical status of clusters. The cluster parameters and mass function (MF) derived using the cluster members would significantly enhance the knowledge of these poorly studied open clusters. These objects are old age OCs and have identical locations in the Galaxy. So, we can compare their dynamic behavior on the position in the Galaxy. We include an orbital analysis of these two candidates for the first time using Gaia EDR3 data. Orbits of OCs are essential to understanding the influence of tides and the formation and evolution processes of the clusters. The primary aim of paper is to select the probable cluster members, obtain the fundamental parameters, binary fraction, the mass function slope, and explain the Galactic orbits of Haffner 22 and Melotte 71 in the Gaia era. The identification maps for both clusters are shown in Figure 1, which is taken from the Leicester Database and Archive Service.

The available information for target clusters is as follows:

Haffner 22: ($\alpha_{2000} = 8^h12^m27^s$, $\delta_{2000} = -27^\circ\ 54'\ 00''$; $l = 246\overset{\circ}{.}775$, $b = 3\overset{\circ}{.}377$) (Dias et al. 2002). Kharchenko et al. (2013) cataloged the proper motions, distance, reddening and log(age) value of Haffner 22 as (−4.52, 6.90) mas yr^{-1}, 2796 pc, 0.21 mag and 9.19, respectively using 2MASS and PPMXL data. Dias et al. (2014) derived proper motion values of this cluster as -1.95 ± 1.80 and 2.67 ± 1.57 mas yr^{-1} based on UCAC4 catalog. A catalog of cluster membership has been provided by Sampedro et al. (2017) based on UCAC4 data. Cantat-Gaudin et al. (2018) has made a catalog for the cluster members and estimated the physical parameters of Haffner 22 based on Gaia DR2 data. We have given comparision table for the fundamental parameters in Table 4.

Melotte 71: ($\alpha_{2000} = 7^h37^m30^s$, $\delta_{2000} = -12^\circ\ 4'\ 00''$; $l = 228\overset{\circ}{.}949$, $b = 4\overset{\circ}{.}498$) (Dias et al. 2002). Sampedro et al. (2017) cataloged the log(age), distance and reddening values as 8.37, 3154 pc and 0.11 mag, respectively. Kharchenko et al. (2013) cataloged the proper motions, distance, reddening and log(age) value of Melotte 71 as (−0.94, 4.72) mas yr^{-1}, 2473 pc, 0.10 mag and 8.97, respectively. Brown et al. (1996) analyzed the high-dispersion echelle spectra for two or three stars in the old anticenter disk cluster Melotte 71 and obtained [Fe/H] value as -0.3 ± 0.2 dex. Mermilliod et al. (1997) have used new CORAVEL radial-velocity observations and *UBV* photometry of 24 red giants in the field of Melotte 71 and obtained mean radial velocity as 50.14 ± 0.14 km s^{-1}. Twarog et al. (2006) have presented a CCD photometry on the intermediate-band *uvbyCaHβ* system for Melotte 71. Interstellar reddening, age and distance modulus have been estimated as 0.20 ± 0.004, 0.9 ± 0.1 Gyr and 12.2 ± 0.1 mag.

Binary stars are a unique tool to gather valuable information about the stellar properties. They play a vital role in the dynamical evolution of star clusters (Sollima 2008). The observational and theoretical works suggest that the stars in clusters may be born originally with large binary fractions, and thus the majority of stars are found in binary systems (Duquennoy & Mayor 1991; Kroupa 1995a, 1995b; Griffin & Suchkov 2003; Goodwin & Kroupa 2005; Kouwenhoven et al. 2005; Rastegaev 2010). Many of the Milky Way's open and globular clusters show a binary fraction with a rising binary frequency toward the cluster core, which is interpreted to be the

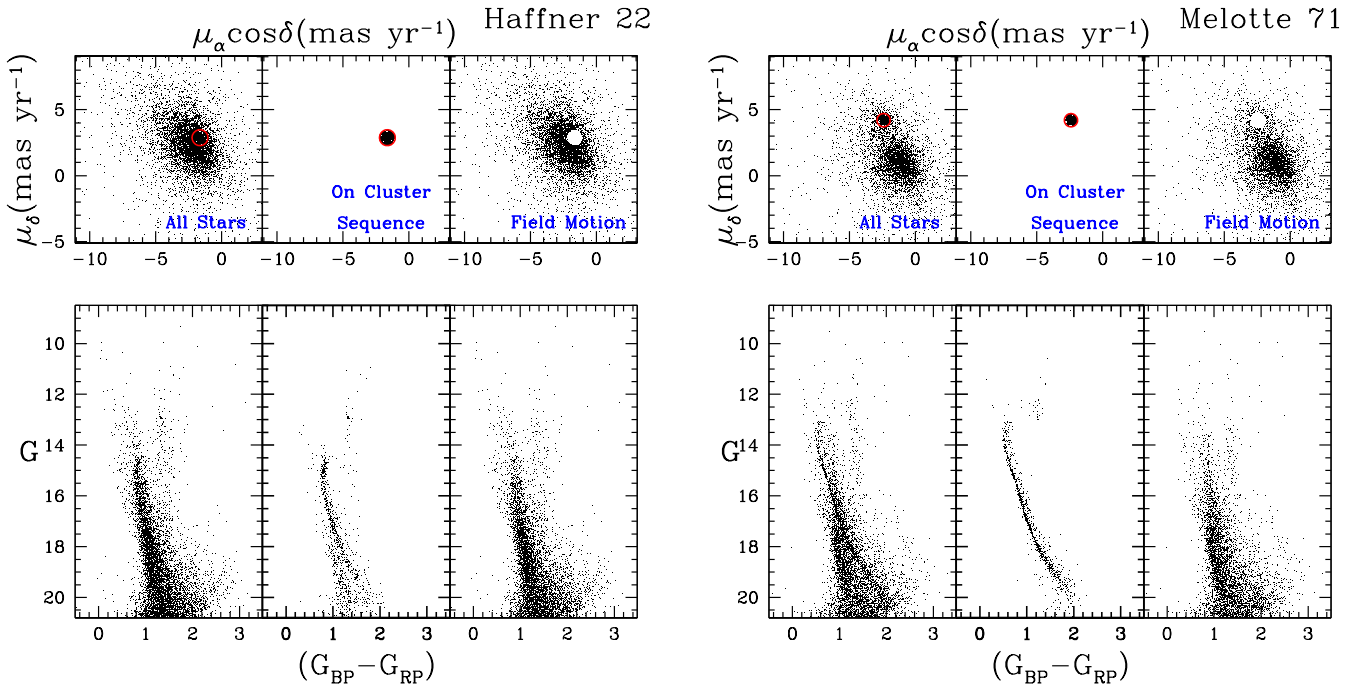

Figure 2. (Top panels) Proper-motion vector point diagrams (VPDs) for Haffner 22 and Melotte 71. (Bottom panels) G versus $(G_{BP} - G_{RP})$ color–magnitude diagrams. (Left panel) The entire sample. (Center) Stars within the circle of 0.6 and 0.5 mas yr^{-1} radius for the clusters Haffner 22 and Melotte 71 centered around the mean proper motion of the cluster. (Right) Probable background/foreground field stars in the direction of this object.

result of mass segregation (e.g., Mathieu & Latham 1986; Geller & Mathieu 2012; Milone et al. 2012). Binary stars can affect the observational parameters of a star cluster, such as the velocity dispersion and the stellar mass function. Therefore, the distribution of the binary fraction in OCs is of crucial importance for several fields in astrophysics.

The outlook of the paper is as follows. Section 2 describes the used data. Section 3 deals with the study of proper motion, determination of distance using parallax, determining the membership probability of stars, and identifying the BSS. The structural properties, derivation of fundamental parameters using the most probable cluster members, and the study of binary fraction in both clusters have been carried out in Section 4. The dynamical analysis of the clusters is discussed in Section 5. The cluster's orbit is studied in Section 6. Finally, the conclusions are presented in Section 7.

2. Data Used

We have used a photometric and astrometric database of 10′ radius circular field from the Gaia EDR3 (Gaia Collaboration et al. 2021) catalog for the clusters Haffner 22 and Melotte 71. No quality cuts have been made in this selection. If we increase our selection radius from 10′ then more members can be found, but this will not change the main results discussed in this paper significantly. The total number of stars within the applied radius were 6172 and 8043 for clusters Melotte 71 and Haffner 22. The main quantities contained by the above catalog are: positions (α, δ), parallaxes and proper motions ($\mu_\alpha \cos\delta$, μ_δ) up to a limiting magnitude of $G = 21$ mag. The uncertainties in the parallax values are ∼0.02–0.03 milliarcsecond (mas) for sources at $G \leqslant 15$ mag and ∼0.07 mas for sources with $G \sim 17$ mag. The uncertainties in the corresponding proper motion components are ∼0.01–0.02 mas yr^{-1} (for $G \leqslant 15$ mag), ∼0.05 mas yr^{-1} (for $G \sim 17$ mag), ∼0.4 mas yr^{-1} (for $G \sim 20$ mag) and ∼1.4 mas yr^{-1} (for $G \sim 21$ mag). In this paper we have used stars upto 20th G mag. Using parallax and proper motion conditions, we have removed 1950 and 1220 stars from Haffner 22 and Melotte 71 respectively.

3. Proper Motions and Field Star Separation

It is required to have precise information about proper motions to differentiate member stars from field stars. We used the kinematical data from the Gaia EDR3 catalog to separate field stars from cluster stars. PMs, $\mu_\alpha\, cos\delta$ and μ_δ are plotted as vector point diagrams (VPDs) in the top panels of Figure 2. The bottom panels show G versus $(G_{BP} - G_{RP})$ CMDs. The left panel in the CMDs shows all-stars present in the cluster's area, while the middle and right panels show the possible cluster members and non-member stars, respectively. By visual inspection, we define the center and radius of the cluster members in VPD for a preliminary analysis. This selection was performed to minimize the field star contamination and keep

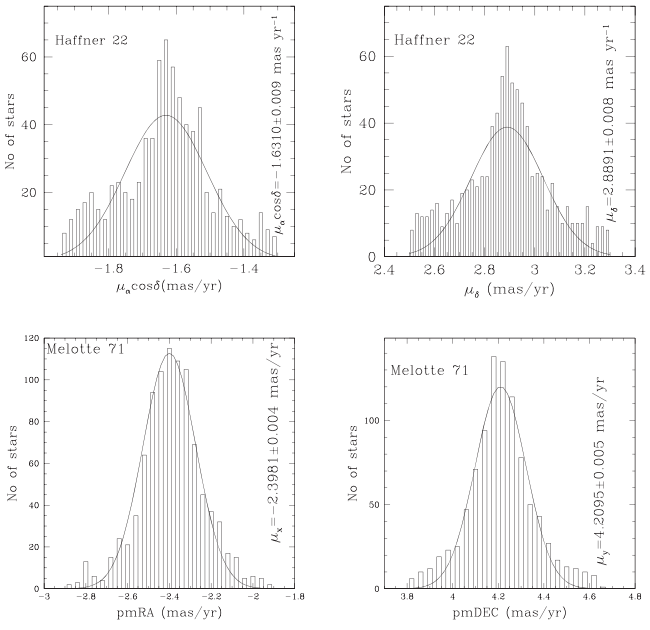

Figure 3. Proper motion histograms of 0.1 mas yr^{-1} bins in R.A. and decl. of the clusters Haffner 22 and Melotte 71. The Gaussian function fit to the central bins provides the mean values in both directions as shown in each panel.

the maximum possible number of lower mass stars. A circle of 0.6 mas yr^{-1} for Haffner 22 while 0.5 mas yr^{-1} for Melotte 71 around the center of the member stars distribution in the VPDs characterize our membership criteria. The picked radius is an agreement between losing cluster members with poor PMs and the involvement of non-member stars. We have also used parallax for the reliable estimation of cluster members. A star is considered a probable cluster member if it lies inside the circle in VPD and has a parallax value within 3σ from the mean cluster parallax. Finally, the main sequence of the cluster is separated. These stars have a PM error of $\leqslant$0.5 mas yr^{-1}.

For the precise estimation of mean proper motion, we deal only with the probable cluster members based on the clusters' VPDs and CMDs as shown in Figure 3. By fitting the Gaussian function on the constructed histograms, we determined the mean proper motion in the directions of R.A. and decl. as $(-1.631 \pm 0.009,\ 2.889 \pm 0.008)$ and $(-2.398 \pm 0.004,\ 4.210 \pm 0.005)$ mas yr^{-1} for Haffner 22 and Melotte 71. From the peak of the Gaussian distribution, we found the mean proper motion in R.A. and decl. directions for both the clusters and are listed in Table 9. The estimated values of mean proper motions for each cluster are in fair agreement with the values given by Liu & Pang (2019) and Cantat-Gaudin et al. (2018). Cantat-Gaudin et al. (2018) catalog report the membership probabilities of stars up to 18th magnitude in the G band for both clusters. We derived membership probabilities of the stars up to 20th magnitude in the G band and the method we used has been discussed in the next section.

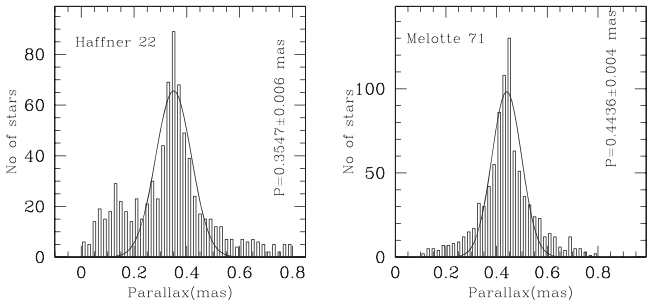

Figure 4. Histogram of parallax for the clusters Haffner 22 and Melotte 71. The Gaussian function fitting to the central bins provides mean value of parallax.

3.1. Distance of Clusters Using Parallax

We have used the parallax of stars to obtain the distance of clusters Haffner 22 and Melotte 71. The Gaia EDR3 parallax has been corrected for these clusters after using zero-point offset (−0.017 mas) as given by Lindegren et al. (2021). The histograms of parallax using probable members in both clusters with 0.15 mas bins are shown in Figure 4. The mean parallax is estimated as 0.3547 ± 0.006 mas and 0.4436 ± 0.004 mas for the clusters Haffner 22 and Melotte 71 and the corresponding distance values (reciprocal of cluster parallax) are 2.82 ± 0.05 kpc and 2.25 ± 0.07 kpc. As listed in Table 4., our obtained value of mean parallax for both objects is very close to the value given by Liu & Pang (2019) and Cantat-Gaudin et al. (2018). We have also used the method discussed by Bailer-Jones et al. (2018) for distance estimation from cluster parallax. Finally, our obtained values are 2.88 ± 0.10 kpc and 2.28 ± 0.15 kpc for the clusters Haffner 22 and Melotte 71, respectively. These values of cluster distance are in fair agreement with the values obtained from the isochrone fitting method as described above. The distances calculated using the trigonometric parallaxes are more accurate as compared to the other techniques because this method is not dependent on the intrinsic properties of the object. As discussed by Bailer-Jones (2015) the parallax data from Gaia have corresponding error values. Which can affect the result if we calculate distances by direct inverting the parallax values. So out of the three distances calculated by us in this article, we prefer the distance obtained by using the method described by Bailer-Jones et al. (2018).

3.2. Membership Probability

Open clusters are located within the densely populated Galactic plane and are usually contaminated by many foreground/background stars. It is required to discriminate between cluster members and non-members to acquire more reliable cluster fundamental parameters. The astrometric membership determination from the Gaia catalog has become more precise than using ground-based data (Dias et al. 2018). We used the

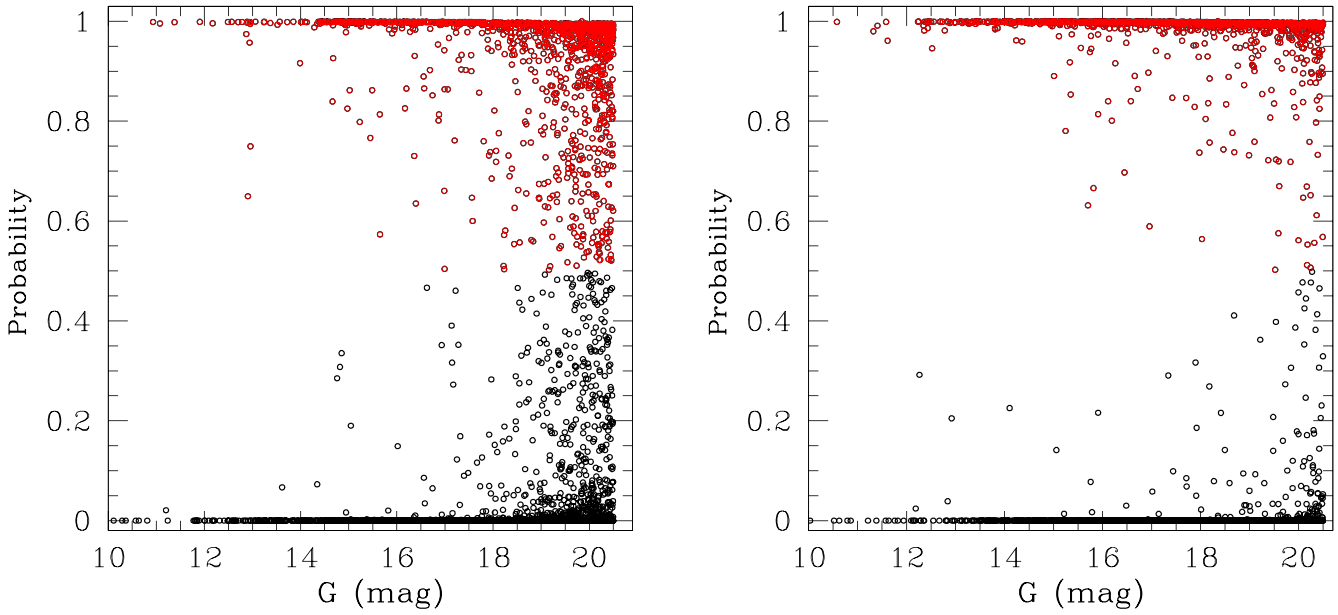

Figure 5. Membership probability as a function of G magnitude. The red circles show the cluster members with membership probability higher than 50% in both the panels.

membership determination method from Balaguer-Núñez et al. (1998) for the clusters Haffner 22 and Melotte 71. Many authors have previously used this method (Bellini et al. 2009; Bisht et al. 2020a, 2020b, 2021a, 2021b; Sariya et al. 2021a, 2021b).

For the cluster and field star distributions, two distribution functions (ϕ_c^ν) and (ϕ_f^ν) are constructed for a particular ith star. The values of frequency distribution functions are given as follows:

$$\phi_c^\nu = \frac{1}{2\pi\sqrt{(\sigma_c^2+\epsilon_{xi}^2)(\sigma_c^2+\epsilon_{yi}^2)}} \times \exp\left\{-\frac{1}{2}\left[\frac{(\mu_{xi}-\mu_{xc})^2}{\sigma_c^2+\epsilon_{xi}^2}+\frac{(\mu_{yi}-\mu_{yc})^2}{\sigma_c^2+\epsilon_{yi}^2}\right]\right\}$$

and

$$\phi_f^\nu = \frac{1}{2\pi\sqrt{(1-\gamma^2)}\sqrt{(\sigma_{xf}^2+\epsilon_{xi}^2)(\sigma_{yf}^2+\epsilon_{yi}^2)}} \times \exp\left\{-\frac{1}{2(1-\gamma^2)}\left[\frac{(\mu_{xi}-\mu_{xf})^2}{\sigma_{xf}^2+\epsilon_{xi}^2} - \frac{2\gamma(\mu_{xi}-\mu_{xf})(\mu_{yi}-\mu_{yf})}{\sqrt{(\sigma_{xf}^2+\epsilon_{xi}^2)(\sigma_{yf}^2+\epsilon_{yi}^2)}}+\frac{(\mu_{yi}-\mu_{yf})^2}{\sigma_{yf}^2+\epsilon_{yi}^2}\right]\right\}$$

where (μ_{xi}, μ_{yi}) are the PMs of ith star. The PM errors are represented by (ϵ_{xi}, ϵ_{yi}). The cluster's PM center is given by (μ_{xc}, μ_{yc}) and (μ_{xf}, μ_{yf}) represent the center of field PM values. The intrinsic PM dispersion for the cluster stars is denoted by σ_c, whereas σ_{xf} and σ_{yf} provide the intrinsic PM dispersion's for the field populations. The correlation coefficient γ is calculated as:

$$\gamma = \frac{(\mu_{xi}-\mu_{xf})(\mu_{yi}-\mu_{yf})}{\sigma_{xf}\,\sigma_{yf}}.$$

Stars with PM errors $\leqslant$0.5 mas yr^{-1} have been used to determine ϕ_c^ν and ϕ_f^ν. A group of stars is found at $\mu_{xc} = -1.631$ mas yr^{-1}, $\mu_{yc} = 2.889$ mas yr^{-1} for Haffner 22 and $\mu_{xc} = -2.398$ mas yr^{-1}, $\mu_{yc} = 4.210$ mas yr^{-1} for Melotte 71. Assuming a distance of 2.90 and 2.30 kpc for the clusters under study and radial velocity dispersion of 1 km s^{-1} for the open star clusters (Girard et al. 1989), the expected dispersion (σ_c) in PMs would be $\sim$0.08 and 0.10 mas yr^{-1} for the clusters Haffner 22 and Melotte 71. For field region stars, we have estimated (μ_{xf}, μ_{yf}) = ($-$2.2, 1.3) mas yr^{-1} for Haffner 22 and (μ_{xf}, μ_{yf}) = ($-$1.5, 0.8) mas yr^{-1} for Melotte 71 and (σ_{xf}, σ_{yf}) = (1.2, 1.9), (2.3, 1.9) mas yr^{-1} for both the objects.

We identified 382 and 597 stars as cluster members for Haffner 22 and Melotte 71 with membership probability higher than 50% and $G \leqslant 20$ mag. In Figure 5, we plotted membership probability versus G magnitude for both the clusters. In Figure 6, we have plotted G versus ($G_{\rm BP} - G_{\rm RP}$) CMD, the identification chart and proper motion distribution using stars with membership probability higher than 50%. In proper motion distribution of clusters, we have plotted field region stars also as shown by black dots.

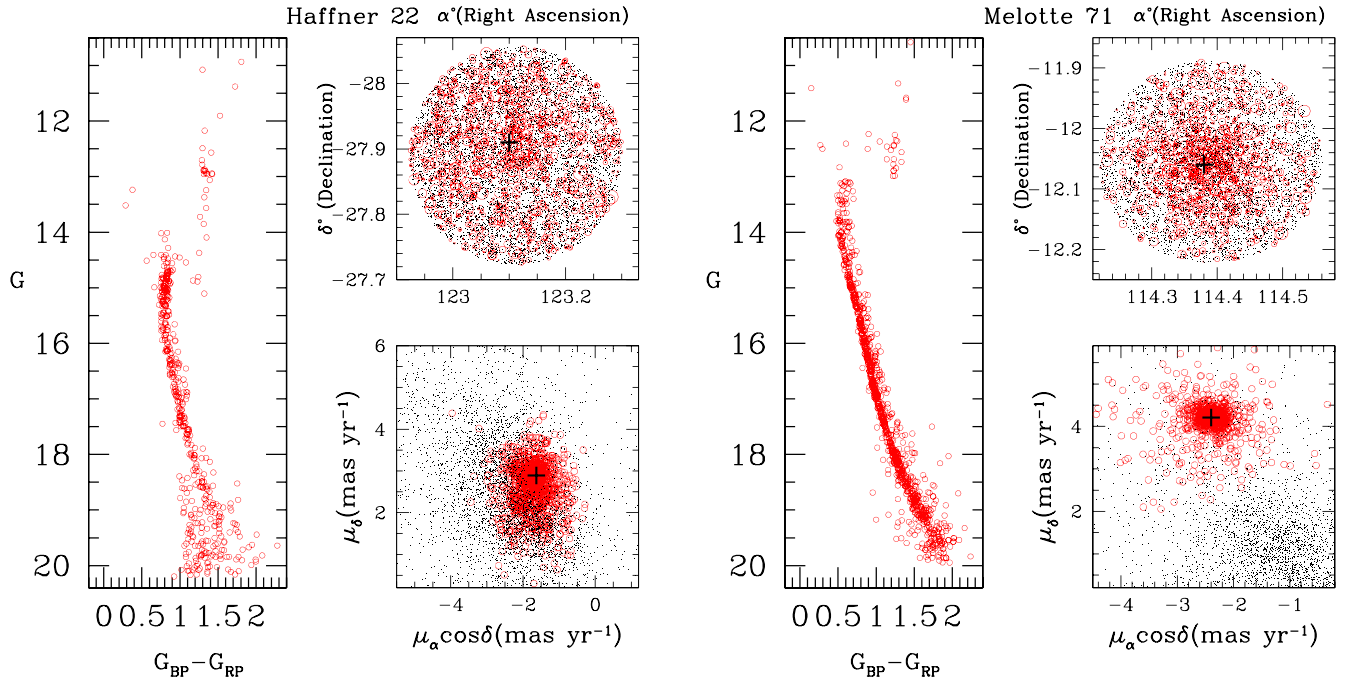

Figure 6. (G, $G_{BP} - G_{RP}$) CMD, identification chart and proper motion distribution of member stars with membership probability higher than 50%. Black dots in proper motion distribution are field stars with membership probability less than 50%. The plus sign indicates the cluster center in position and proper motions.

Membership probability has been determined for the clusters Haffner 22 and Melotte 71 by Cantat-Gaudin et al. (2018) up to 18.0 mag using the Gaia-DR2 catalog. To make a comparison on membership probability, we have plotted G, $G_{BP} - G_{RP}$ CMDs using our membership catalog and Cantat-Gaudin et al. (2018) catalog as shown in Figure 7. We used only probable members with membership probability higher than 50%. Our membership determination is clearly atleast 2 magnitude deeper than Cantat-Gaudin et al. (2018). This enhances our precision in determining various parameters of star clusters, varying from distance, extinction, and mass function.

3.3. Determination of the Effectiveness of Probabilities

We can not avoid the contamination of background/foreground stars through the observational projection effect. We can review quantitatively how adequate the results of our membership estimation were.

To ascertain the effectiveness of our membership determination, we used the expression given by Shao & Zhao (1996):

$$E = 1 - \frac{N \times \Sigma[P_i(1 - P_i)]}{\Sigma P_i \Sigma(1 - P_i)}$$

where N is the total number of stars with membership probability higher than 50% and Pth indicates the probability of ith star of the cluster. We obtained the effectiveness (E) values as 0.48 and 0.51 for the clusters Haffner 22 and Melotte 71. Shao & Zhao (1996) calculated the effectiveness of membership determination for 43 OCs as ranges from 0.20 to 0.90 with a peak value of 0.55. Our estimated values of the effectiveness of membership determination are lying within the above range and approaching a slightly higher side as well.

3.4. Blue Straggler Stars

The BSS are intriguing objects present in the stellar environments like the clusters (Johnson & Sandage 1955; Sandage 1962; Ahumada & Lapasset 1995.) In Brief, it has been recommended that BSS are the result of stellar collisions (Benz & Hills 1987; Lombardi et al. 1996) or because of the mass exchange in close binary systems (McCrea 1964; Eggen & Iben 1989; Mateo et al. 1990). The second-generation stars (Eggen & Iben 1988), accretion of gas from the surrounding interstellar medium (Williams 1964), and capture of non-member stars by a star cluster are other suggested aspects behind the formation of BSS in stellar systems. BSS are stars lying above the main sequence (MS) turnoff region in color–magnitude diagrams (CMDs). If the BSS had been normal single stars, they should already have evolved away from the MS (Stryker 1993). In the 1990s, early studies gave the first hints for BSS showing this effect in GCs and some OCs (Auriere et al. 1990; Mathieu & Latham 1986). This paper found five and four-member BSS in clusters Haffner 22 and Melotte 71, respectively. Those BSS members are located at a radial distance of ∼0′.6–6′.5 and ∼0′.6–9′.8 for Haffner 22 and Melotte 71, respectively. We imply that the BSSs are lying in

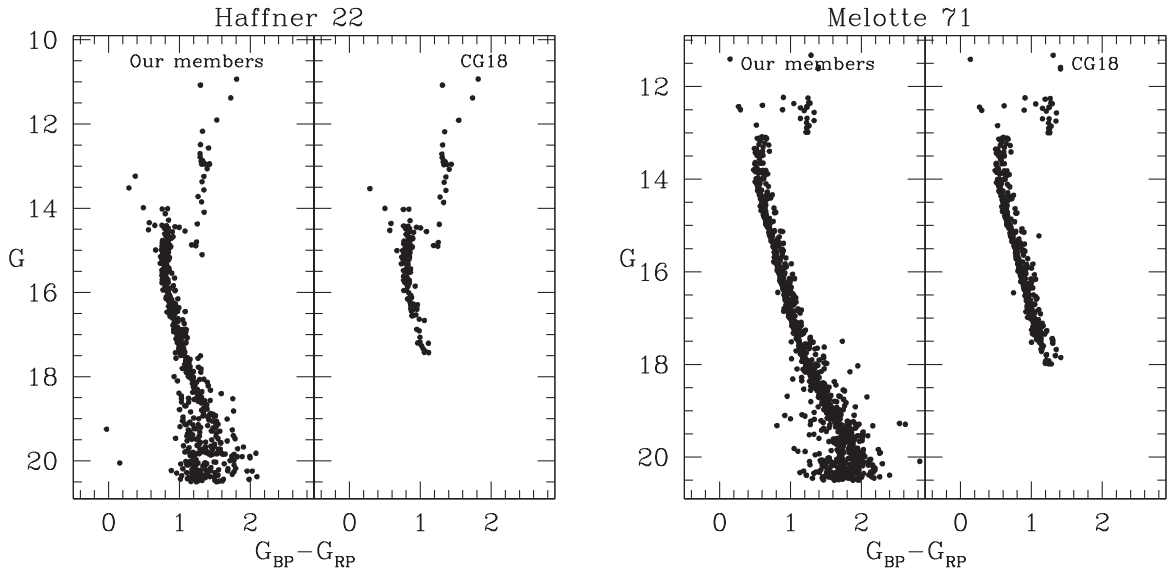

Figure 7. The (G, $G_{BP} - G_{RP}$) CMDs of our identified members and members from Cantat-Gaudin et al. (2018) (CG18) catalog. All the stars plotted here have a membership probability higher than 50%.

Table 1
The Identified BSS Candidates in the Cluster Haffner 22

GaiaEDR3	R.A. (deg)	Decl. (deg)	pmRA (mas yr^{-1})	pmDEC (mas yr^{-1})	plx (mas)	Gmag (mag)	Bp–Rp (mag)	r (arcmin)	prob
5693065398100156800	123.14114760440	−27.95287418172	−1.562	2.814	0.3872	13.237711	0.3767	4.0767	0.99
5692972077053132288	123.03294244320	−27.97111049151	−1.584	3.042	0.3496	13.518732	0.2865	6.4224	0.99
5693817189175756032	123.08835909476	−27.89216823376	−1.872	2.861	0.2917	13.988064	0.4903	1.2604	0.91
5693817601492594176	123.08188716773	−27.85595962460	−1.703	3.010	0.2733	14.345200	0.5744	2.5928	0.99
5693817257895191424	123.11862294354	−27.88077803456	−1.569	2.892	0.3236	14.513340	0.5620	0.6554	0.99

Table 2
The Identified BSS Candidates in the Cluster Melotte 71

GaiaEDR3	R.A. (deg)	Decl. (deg)	pmRA (mas yr^{-1})	pmDEC (mas yr^{-1})	plx (mas)	Gmag (mag)	Bp–Rp (mag)	r (arcmin)	prob
3033959198481332736	114.40683348610	−12.06451836239	−2.242	4.290	0.4837	11.408119	0.1468	1.1409	0.99
3033956307964730880	114.23005068396	−12.09950761098	−2.600	2.077	0.3975	12.348255	0.2989	9.7571	0.98
3033962183479250432	114.39487869798	−12.04600820646	−2.209	4.220	0.4588	12.432313	0.2667	0.6109	0.99
3033962664515580672	114.39443602193	−11.99131028286	−2.392	4.281	0.4300	12.500945	0.2947	3.8302	0.90

the outer region for these clusters, which could form because of binarity. Our analysis suggests that all the identified BSS are confirmed cluster members with a membership probability higher than 90%. We have plotted all the member BSS in Figure 10 for both clusters by blue solid dots. All the identified BSS for Haffner 22 and Melotte 71 are listed in Tables 1 and 2 respectively. Five BSS have previously been identified by Rain et al. (2021) in the cluster Melotte 71. We have cross-matched our BSS with Rain et al. (2021) and found that three members (Gaia source IDs- 3033959198481332736, 3033962183479250432, and 3033962664515580672) are matched. The other two members do not lie in our field of view for Melotte 71. The BSS of Haffner 22 are not cataloged in the literature.

4. Fundamental Parameters of the Clusters

4.1. Cluster Center and Radial Density Profile

In the earlier investigations of the open clusters, the center used to be determined just by the visual inspection

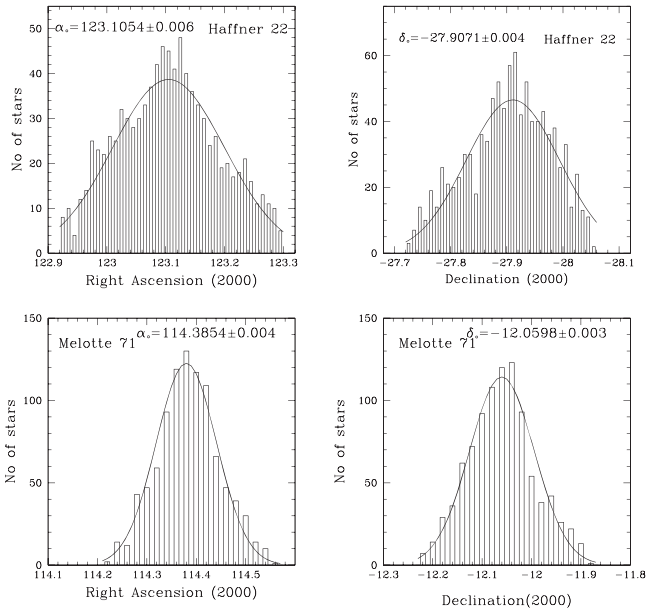

Figure 8. Profiles of stellar counts across the region of clusters Haffner 22 and Melotte 71. The Gaussian fits have been applied. The center of symmetry about the peaks of R.A. and decl. is taken to be the position of cluster's center.

(Becker & Fenkart 1971; Romanishim & Angel 1980). To present the precise measurement of the fundamental parameters in clusters Haffner 22 and Melotte 71, we used the star-count method using stars with membership probability higher than 50%. Figure 8 represents the histograms for both clusters in R. A. and decl. directions. The Gaussian curve-fitting is performed to the star count profiles, and the estimated center coordinates are listed in Table 9. Our evaluation is in good agreement with the values given by Dias et al. (2002). and Cantat-Gaudin et al. (2018).

We have plotted the radial density profile (RDP) for Haffner 22 and Melotte 71 using the above-estimated center coordinates. The cluster area is divided into many concentric rings around the core having an equal additional radius. The number density, ρ_i, in the ith zone is determined by using the formula, $\rho_i = \frac{N_i}{A_i}$, where Nth is the number of cluster members, and Ath is the area of the ith zone. We obtained the radii of the clusters based on the visual inspection from RDPs. According to our criteria, the radius is the point after that cluster density merges with the field density. The errors in background density levels are also shown by the dashed lines in Figure 9. We considered 5′.5 and 6′.5 as the cluster radius for the clusters Haffner 22 and Melotte 71. Our estimated radius value for Haffner 22 is slightly less than the value of Carraro et al. (2016). We obtained the radius of Melotte 71 is higher than the value cataloged by Dias et al. (2014). The enhancement of radius around 3′.5 below 2σ for cluster Haffner 22 indicates the presence of a possible corona region for this object. The appearance of the corona region may be because of two main reasons: the mass-segregation effect in this object (Nilakshi & Sagar 2002), and the corona of the clusters is molded by the Galactic tidal fields (Mathieu 1985). To estimate the spatial parameters, we fitted the King (1962) model as shown by the continuous black curve in Figure 9. The King (1962) profile is given by:

$$f(r) = f_b + \frac{f_0}{1 + (r/r_c)^2}$$

where r_c , f_0 , and f_b are the core radius, central density, and the background density level, respectively. By fitting the King model to RDPs, we have derived the structural parameters for both the clusters as listed in Table 3. The density contrast parameter ($\delta_c = 1 + \frac{f_0}{f_b}$) is calculated for both the clusters under study using the member stars selected from proper motion data. We obtained the value of density contrast parameter (δ_c) as 5.3 and 14.1 for Haffner 22 and Melotte 71. Our estimated value for Haffner 22 is lower than the limit ($7 \leqslant \delta_c \leqslant 23$) as given by Bonatto & Bica (2009), which suggests that Haffner 22 is a sparse cluster. Our obtained value of δ_c for Melotte 71 is lying within the limit given by Bonatto & Bica (2009), which suggests that this cluster is compact. We have also estimated the limiting radius ($r_{\rm lim}$) and concentration parameter (c) for both the clusters, which are listed in Table 3.

It is very well known that every cluster consists of mainly two regions, core and corona (Nilakshi et al. 2002). We can describe these two regions using clusters RDP. In Haffner 22, we can see the enhancement of radius around 3′.5. This may be because of the presence of a possible corona region in this object.

4.2. Age and Distance

To trace the Galaxy's Galactic structure and chemical evolution using OCs, the distance and age of OCs play the most crucial role (Friel & Janes 1993). We have estimated the mean value of A_G for the clusters Haffner 22 and Melotte 71 as 0.63 ± 0.18 and 1.40 ± 0.35 using probable members from Gaia DR2 data. We obtained the main fundamental parameters (age, distance, and reddening) by fitting the isochrones with metallicity $Z = 0.005$ for Haffner 22 and $Z = 0.008$ for Melotte 71 of Marigo et al. (2017) to the G, $G_{\rm BP} - G_{\rm RP}$ CMD as shown in Figure 10. Our used metallicity for Melotte 71 is very close to the value $Z = 0.007$ as given by Brown et al. (1996). The above-used isochrones are derived from the stellar evolutionary tracks computed with PARSEC (Bressan et al. 2012) and COLIBRI (Marigo et al. 2013) codes.

The estimation of the main fundamental parameters for the clusters are given below:

Haffner 22: We fitted the theoretical isochrones of different ages (log(age) = 9.30, 9.35 and 9.40) in all the CMDs for the cluster Haffner 22, shown in Figure 10. The best global fit is

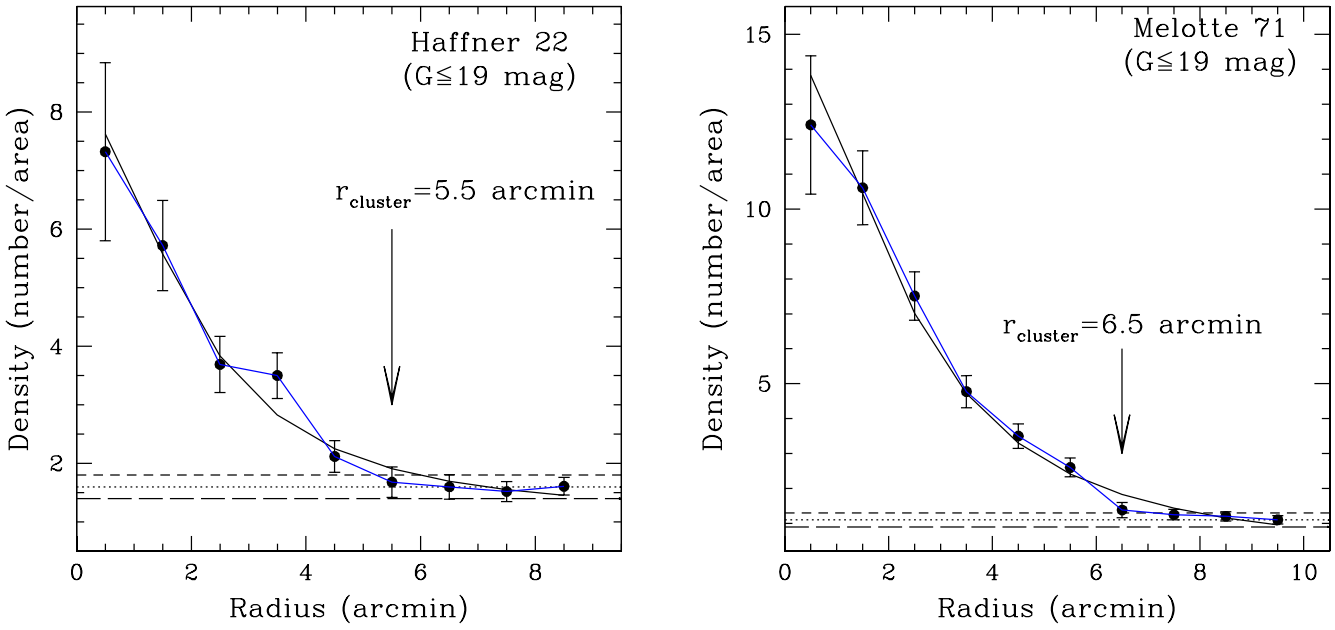

Figure 9. Surface density distribution of the clusters Haffner 22 and Melotte 71. Errors are determined from sampling statistics ($=\frac{1}{\sqrt{N}}$ where N is the number of cluster members used in the density estimation at that point). The smooth line represent the fitted profile of King (1962) whereas dotted line shows the background density level. Long and short dash lines represent the errors in background density.

Table 3
Structural Parameters of the Clusters Under Study

Name	f_0	f_b	r_c (arcmin)	r_c (parsec)	δ_c	$r_{\rm lim}$ (arcmin)	c	R_t (parsec)
Haffner 22	6.94	1.60	2.1	1.7	5.3	7.2	0.55	12.19
Melotte 71	14.34	1.10	2.4	1.6	14.1	11.6	0.68	15.13

Note. Background and central density are in the unit of stars per arcmin^2. Core radius (r_c) and tidal radius (R_t) are in arcmin and pc.

favorable for the middle isochrone with log(age) = 9.35 to the high mass cluster members. A good fitting of isochrones provides an age of 2.25 ± 0.25 Gyr. Our obtained value of age is close to the value cataloged by Kharchenko et al. (2013). The apparent distance modulus ($(m-M) = 12.80 \pm 0.4$ mag) provides a distance of 2.8 ± 0.50 kpc from the Sun. Our calculated value of the distance shows good agreement with the values obtained by Cantat-Gaudin et al. (2020) and Kharchenko et al. (2013).

Melotte 71: The isochrones of different ages (log(age) = 9.05, 9.10 and 9.15) have been overplotted on all the CMDs for the cluster Melotte 71 as shown in Figure 10. The overall fit is satisfactory for log(age) = 9.10 (middle isochrone) to the brighter stars, corresponding to 0.8 ± 0.1 Gyr. The estimated value of age is very close to the value cataloged by Sampedro et al. (2017). The estimated distance modulus ($(m-M) = 13.30 \pm 0.3$ mag) provides a distance from the Sun that is 2.5 ± 0.20 kpc. Our obtained value of the distance is in fair agreement with the value given by Kharchenko et al. (2016).

The galactocentric coordinates of the clusters X (directed toward the galactic center in the Galactic disk), Y (directed toward the Galactic rotation), and distance from the galactic plane Z (directed toward the Galactic north pole) can be estimated using clusters' distances, longitude, and latitude. The Galactocentric distance has been calculated by considering 8.3 kpc (Bajkova & Bobylev 2016) as the distance of Sun to the Galactic center. The estimated Galactocentric coordinates are listed in Table 9. Our obtained values of the Galactocentric coordinates are in fair agreement with the values obtained by Cantat-Gaudin et al. (2018). We have compared our estimated parameters with the previously published values in the literature for both clusters. Table 4 presents the comparison table for the clusters Haffner 22 and Melotte 71. All the estimated parameters are comparable with the literature values.

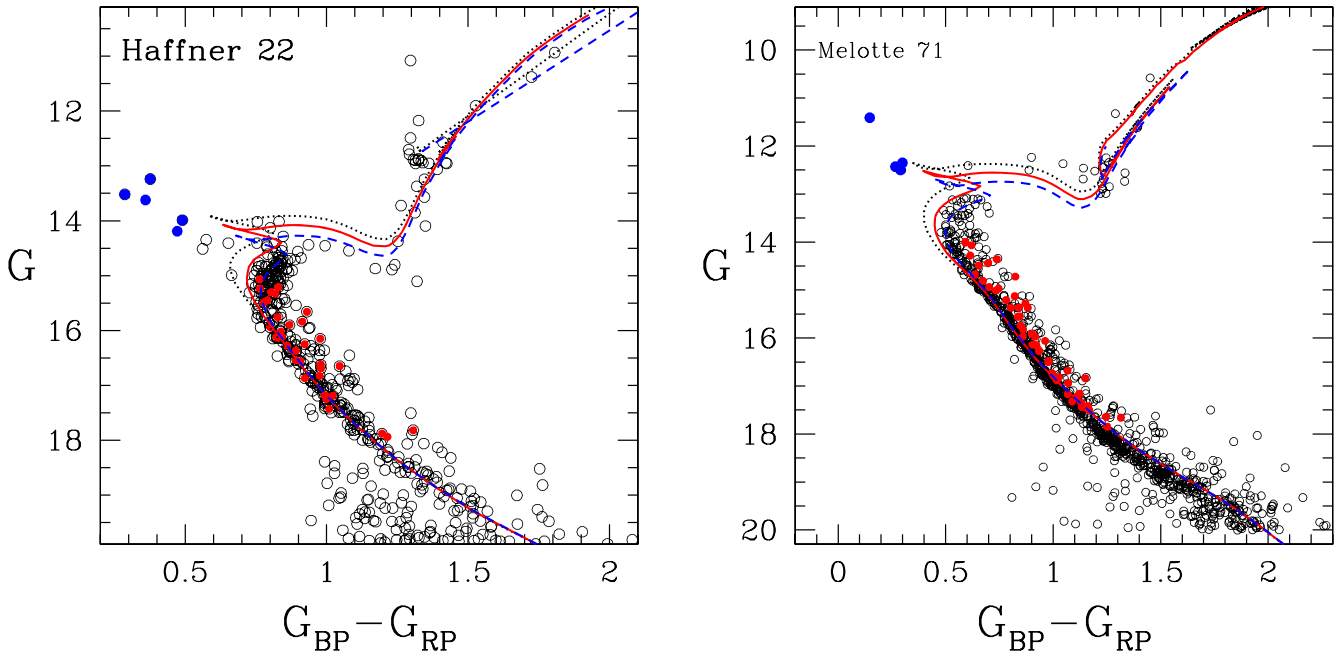

Figure 10. The color–magnitude diagram of the clusters under study. All stars are probable members with membership probability higher than 50%. The curves are the isochrones of (log(age) = 9.30 , 9.35 and 9.40)) for Haffner 22 and (log(age) = 9.05, 9.10 and 9.15) for Melotte 71. These ishochrones of metallicity $Z = 0.005$ for Haffner 22 and $Z = 0.008$ for Melotte 71 are taken from Marigo et al. (2017). Blue solid dots are the possible member BSS while red dots are identified binary stars.

4.3. Binary Fraction in Clusters

The stellar binary fraction in star clusters is a key factor in understanding the e?ects of binary stars on the properties and dynamical evolution of the host cluster. We have plotted histograms using the tangential velocity of member stars of the clusters Haffner 22 and Melotte 71 as shown in Figure 11. The radius of core and off-core regions are (2′.1 and 3′.4) and (2′.4 and 4′.1) for clusters Haffner 22 and Melotte 71, respectively. In this figure, we found two different peaks for single star and binary star distribution (Bica & Bonatto 2005). In this analysis, we have used main-sequence stars with $15 \leqslant G \leqslant 18$ mag for Haffner 22 and $14 \leqslant G \leqslant 18$ mag for Melotte 71. We have used the weighted mean method to compute the mean value of velocity in core and off- core regions. In the core region, there are 96 stars (1st peak) and 14 stars (2nd peak), and in the off core region, there are 284 stars (1st peak) and 20 stars (2nd peak) for Haffner 22. In the core region, there are 140 stars (1st peak) and 13 stars (2nd peak), and in the off core region, there are 284 stars (1st peak) and 18 stars (2nd peak) for Melotte 71. We estimated the mean value of tangential velocity in core and off-core regions as $(45.04 \pm 6.25,\ 44.99 \pm 6.16)$ km s^{-1} and $(37.38 \pm 2.87,\ 37.60 \pm 3.80)$ km s^{-1} for clusters Haffner 22 and Melotte 71, respectively. We also have obtained the corresponding dispersion in core and off-core region as $(5.4 \pm 2.2,\ 5.3 \pm 2.1)$ km s^{-1} and $(4.9 \pm 1.8,\ 3.7 \pm 1.2)$ km s^{-1} for both clusters. Our estimated values of mean and dispersion for a single star and double star distribution is approximately similar in core and off-core regions for both clusters. This analysis suggests that some binary content is present in both objects. The binary fraction (f_{bin}) in a cluster can be estimated by dividing the number of high-velocity stars by the total number of stars. Thus, in the core region, the binary fractions of Haffner 22 and Melotte 71 are found as $f_{\rm bin} = 13.59 \pm 3\%$ and $14.20 \pm 5\%$. In the off-core region the binary fraction found as $f_{\rm bin} = 11.10 \pm 4\%$ and $10.0\% \pm 6\%$ for both objects. From here, we obtained that binary fraction is more in the core region for both clusters. Bica & Bonatto (2005) have found a higher binary fraction in the core region for OCs NGC 2287, M 48, NGC 6208, NGC 3680, and IC 4651. The total binary fractions are found as $f_{\rm bin} = 12.34\% \pm 3.5\%$ and $12.10\% \pm 5.5\%$ clusters Haffner 22 and Melotte 71, respectively. We have shown all the possible binary stars in Figure 10.

5. Dynamical Study of the Clusters

5.1. Luminosity Function and Mass Function

The luminosity function (LF) and mass function (MF) depend on the number of actual cluster members, and both measures are associated with the well-known mass–luminosity relationship. We used G versus $(G_{\rm BP} - G_{\rm RP})$ CMDs to see the distribution of stars with magnitude in both clusters. The distance modules can convert the G magnitudes of main-sequence stars into absolute

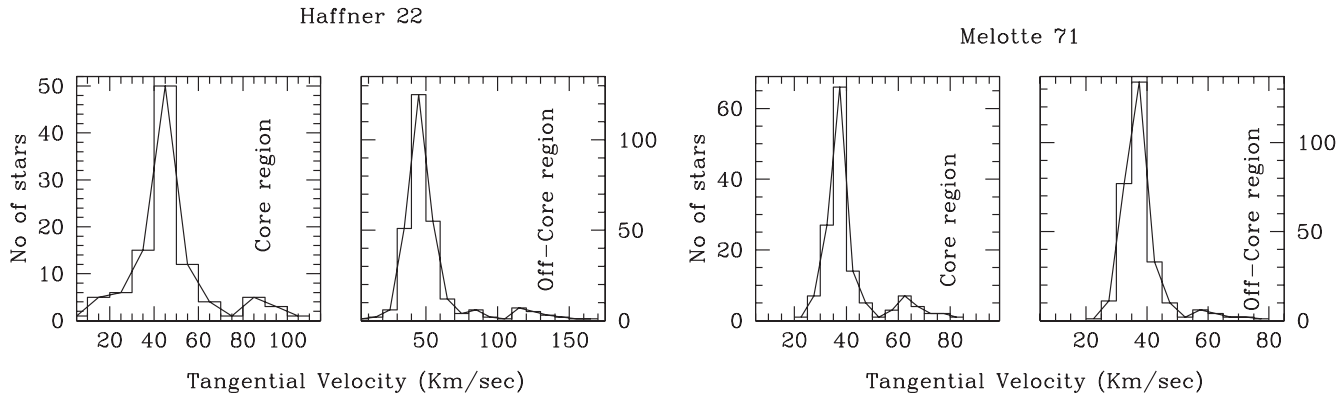

Figure 11. Histograms of tangential velocity in the core (left panels) and off-core (right panels) regions for clusters Haffner 22 and Melotte 71. We have used the individual distances of each star to transform proper motion into tangential velocity. Higher and lower peak in core and off-core regions are showing single star and binary star distribution.

Table 4
A Comparison of our Obtained Fundamental Parameters for the Clusters Haffner 22 and Melotte 71 with the Literature Values

Parameters	Haffner 22	Reference	Melotte 71	Reference
(Right ascension, decl.) (deg)	(123.1054, −27.9071)	*Present study*	(114.3854, −12.0598)	*Present study*
	(123.108, −27.913)	Cantat-Gaudin et al. (2018)	(114.375, −12.069)	Liu & Pang (2019)
	(123.112, −27.90)	Dias et al. (2014)	(114.383, −12.065)	Cantat-Gaudin et al. (2018)
	(123.112, −27.89)	Kharchenko et al. (2013)	(114.375, −12.066)	Sampedro et al. (2017)
			(114.375, −12.06)	Dias et al. (2014)
			(114.390, −12.055)	Kharchenko et al. (2013)
($\mu_\alpha\, cos(\delta)$) (mas yr^{-1})	-1.631 ± 0.009	*Present study*	-2.398 ± 0.004	*Present study*
(μ_δ) (mas yr^{-1})	2.889 ± 0.008	*Present study*	4.210 ± 0.005	*Present study*
	(−1.765, 2.779)	Liu & Pang (2019)	(−2.445, 4.201)	Liu & Pang (2019)
	(−1.638, 2.878)	Cantat-Gaudin et al. (2018)	(−2.446, 4.210)	Cantat-Gaudin et al. (2018)
	(−1.95, 2.67)	Dias et al. (2014)	(−5.07, 5.76)	Dias et al. (2014)
	(−4.52, 6.90)	Kharchenko et al. (2013)	(−0.94, 4.72)	Kharchenko et al. (2013)
Age (log)	9.35	*Present study*	9.10	*Present study*
	9.39	Cantat-Gaudin et al. (2020)	9.06	Liu & Pang (2019)
	9.34	Liu & Pang (2019)	9.11	Bossini et al. (2019)
	9.55	Sampedro et al. (2017)	8.37	Sampedro et al. (2017)
	9.19	Kharchenko et al. (2013)	8.97	Kharchenko et al. (2016)
Radius (arcmin)	5.5	*Present study*	6.5	*Present study*
	6.7	Carraro et al. (2016)	4.5	Dias et al. (2014)
Parallax (mas)	0.3547 ± 0.006	*Present study*	0.4436 ± 0.004	*Present study*
	0.325	Liu & Pang (2019)	0.44	Liu & Pang (2019)
	0.329	Cantat-Gaudin et al. (2018)	0.43	Cantat-Gaudin et al. (2018)
Distance (Kpc)	2.88 ± 0.10	*Present study*	2.28 ± 0.15	*Present study*
	2.802	Cantat-Gaudin et al. (2020)	2.7	Cantat-Gaudin et al. (2018)
	2.344	Sampedro et al. (2017)	3.154	Sampedro et al. (2017)
	3.05	Carraro et al. (2016)	2.473	Kharchenko et al. (2016)
	2.796	Kharchenko et al. (2013)		

magnitudes. We have constructed the histogram of LF with 1.0 mag intervals as shown in Figure 12. This figure exhibits that the LF continues to increase up to $M_G \sim 2.5$ and 3.3 mag for the clusters Haffner 22 and Melotte 71. We have shown the used magnitude limit in Figure 12 using the verticle dotted line.

To convert luminosity into masses, we have employed the theoretical isochrones of Marigo et al. (2017). To understand the MF, we have transformed absolute mag bins to mass bins, and the resulting present-day mass function (PDMF) is shown in Figure 13. The first and last bin is not in the same trend because we have used the fitting error, and the error is higher in

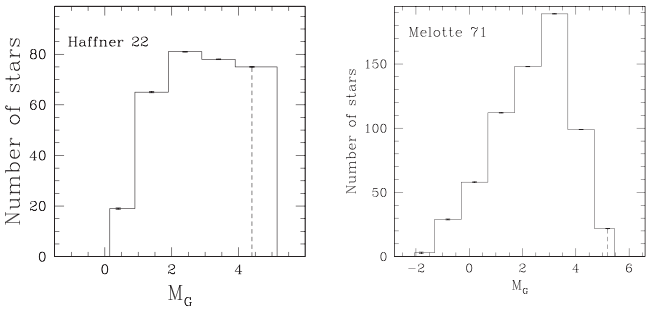

Figure 12. Luminosity function of stars in the region of Haffner 22 and Melotte 71. Verticle dotted line indicates our magnitude limit.

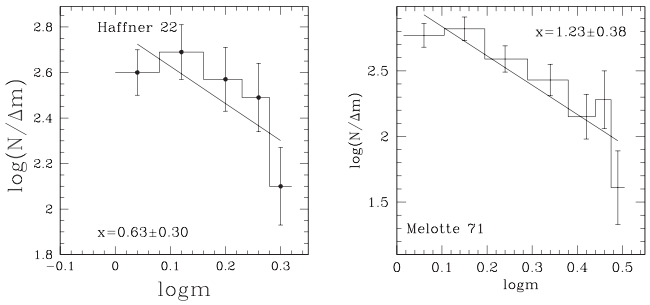

Figure 13. Mass function histogram derived using the most probable members, where solid line indicates the power law given by Salpeter (1955). The error bars represent $\frac{1}{\sqrt{N}}$.

the last bin. The shape of the PDMF of members in Haffner 22 and Melotte 71 for masses $\geqslant 1\ M_{\rm sol}$ can be approximated by a power law of the form

$$\log \frac{dN}{dM} = -(1 + x)\log(M) + \text{constant}$$

Where dN is the number of the probable cluster members in a mass bin dM with central mass M and x is mass function slope. Since Gaia data (G mag) is not complete below G = 19 mag (Arenou et al. 2018), we took only the stars brighter than this limit, which corresponds to stars more massive than 1 $M_{\odot}$. The computed values of the MF slopes are 0.63 ± 0.30 and 1.23 ± 0.38 for the clusters Haffner 22 and Melotte 71, respectively. The MF slope value for Haffner 22 is flatter, while Melotte 71 is satisfactory with the Salpeter's initial mass function slope within error. The dynamical study of Haffner 22 shows a lack of faint stars in the inner region which leads to the mass-segregation effect. In the literature there are many dynamical studies that suggest lack of faint stars toward the center of the cluster (Fischer et al. 1998; Pandey et al. 1992, 2001, 2005; Kumar et al. 2008). The complete mass has been evaluated for both clusters using the derived mass function slope. All the MF-related parameters in this section,

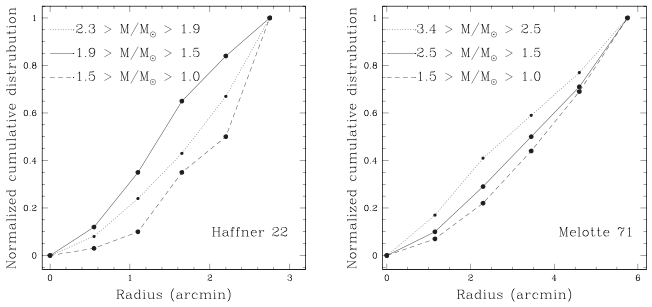

Figure 14. The cumulative radial distribution of stars in various mass range.

Table 5
The Main Mass Function Parameters in Clusters

Object	Mass range $M_{\odot}$	MF slope	Total mass $M_{\odot}$	Mean mass $M_{\odot}$
Haffner 22	1.0–2.3	0.63 ± 0.30	572	1.49
Melotte 71	1.0–3.4	1.23 ± 0.38	1015	1.70

Table 6
Distribution of Stars in Different Mass Ranges Along with the Percentage of Confidence Level in Mass-segregation Effect for the Clusters

Object	Mass range $M_{\odot}$	Confidence level %
Haffner 22	2.3 – 1.9, 1.9 – 1.5, 1.5 – 1.0	88
Melotte 71	3.4 – 2.5, 2.5 – 1.5, 1.5 – 1.0	80

like mass range, mass function slope, and the total mass measured, are listed in Table 5.

5.2. Mass-segregation Study

In mass segregation, the bright stars move toward the cluster center while the low mass stars move toward the halo region (Mathieu 1984; Kroupa 1995; de La Fuente Marcos 1996). Many authors have addressed this phenomenon in clusters (e.g., Hillenbrand & Hartmann 1998; Meylan 2000; Baumgardt & Makino 2003; Dib et al. 2018; Alcock & Parker 2019; Dib & Henning 2019; Bisht et al. 2020b, 2021b). We have used only the probable members to explain the mass segregation effect in our target clusters. We distributed cluster members into three mass ranges as shown in Table 6. The cumulative radial stellar distribution of cluster members for the clusters Haffner 22 and Melotte 71 is shown in Figure 14. This diagram exhibits that the cluster members show a mass segregation effect as bright stars seem to be more centrally concentrated than the low mass members. We found the confidence level of mass segregation is 88% and 80% for the clusters Haffner 22 and Melotte 71, respectively, based on the Kolmogorov–Smirnov ($K - S$) test.

The plausible reason for this effect may be dynamical evolution, an imprint of star formation, or both (Dib et al. 2007; Allison et al. 2009; Pavlik 2020). Our target objects are old-age OCs. So, the possible reasons could be both of these. The relaxation time (T_R) is represented as the time in which the stellar velocity distribution converts Maxwellian and denoted by the following formula (Spitzer & Hart 1971):

$$T_R = \frac{8.9 \times 10^5 \sqrt{N} \times R_h^{3/2}}{\sqrt{\bar{m}} \times \log(0.4N)}$$

where N represents the cluster members with membership probability higher than 50%, R_h is the cluster half mass–radius expressed in parsec and $\bar{m}$ is the average mass of the cluster members (Spitzer & Hart 1971) in the solar unit. The value of $\bar{m}$ is found as 1.49 and 1.70 $M_\odot$ for these objects.

We have estimated the value of R_h based on the transformation equation as given in Larsen (2006),

$$R_h = 0.547 \times R_c \times \left(\frac{R_t}{R_c}\right)^{0.486}$$

where R_c is core radius while R_t is tidal radius. We obtained the value of half light radius as 2.45 and 2.62 pc for the clusters Haffner 22 and Melotte 71, respectively.

The value of dynamical relaxation time T_R is Obtained as 25 and 30 Myr for these objects. Hence, we conclude that Haffner 22 and Melotte 71 are dynamically relaxed OCs.

6. Orbit Study of the Clusters

The study of orbits is beneficial to understand stars, clusters, and Galaxies' formation and evolution processes. We used the Allen & Santillan (1991) criteria for Galactic potentials to obtain Galactic orbits of Haffner 22 and Melotte 71. Bajkova & Bobylev (2016) and Bobylev et al. (2017) have refined Galactic potential model parameters with the help of new observational data for the galactocentric distance $R \sim$ 0–200 kpc. The equations considered for the used models are described by Rangwal et al. (2019). The main fundamental parameters (cluster center (α and δ), mean proper motions ($\mu_\alpha \cos\delta$, μ_δ), parallax, age and heliocentric distance ($d_\odot$)) have been used to determine the orbital parameters in the clusters under study. We have used the radial velocity values as 33.23 ± 0.16 km s^{-1} and 51.26 ± 0.36 km s^{-1} for Haffner 22 and Melotte 71 as taken from the catalog given by Soubiran et al. (2018).

We have transformed equatorial space and velocity components into Galactic-space velocity components. The Galactic center is considered at ($17^h45^m32\overset{s}{.}224$, $-28°56'10''$) and the North-Galactic pole is considered at ($12^h51^m26\overset{s}{.}282$, $27°7'42\overset{''}{.}01$) (Reid & Brunthaler 2004). To apply a correction for Standard Solar Motion and Motion of the local standard of rest (LSR), we used position coordinates of Sun as (8.3,0,0.02) kpc and its velocity components as (11.1, 12.24, 7.25) km s^{-1} (Schonrich et al. 2010). Transformed parameters in Galactocentric coordinate system are listed in Table 7.

Figure 15 shows the orbits of the clusters Haffner 22 and Melotte 71. The left panel of this figure indicates the motion of the cluster in terms of distance from the Galactic center and Galactic plane and this shows a 2D side view of the orbits. In the middle panel, the cluster motion is described in terms of x and y components of Galactocentric distance, which shows a top view of orbits. The right panel of this figure indicates the motion of clusters under study in the Galactic disk with time. Both clusters follow a boxy pattern according to our analysis. Our obtained values of eccentricity are nearly zero for both objects, which demonstrates that the target clusters trace a circular path around the Galactic center. The birth and present day position in the Galaxy are represented by filled circle and triangle as shown in Figure 15. The various orbital parameters have been obtained for these clusters, which are listed in Table 8. Here e is eccentricity, R_a is the apogalactic distance, R_p is perigalactic distance, $Z_{\max}$ is the maximum distance traveled by cluster from Galactic disk, E is the average energy of orbits, J_z is z component of angular momentum, T_R is time period of the revolution around the Galactic center and T_Z is the time period of vertical motion.

In these figures, we can see that the birth positions of both the clusters are in the thick disk of the Galaxy hence not affected by the thin disk and its tidal forces. Also, both the clusters are orbiting outside the solar circle hence not interacting with the inner region of the Galaxy. The disruption of both the clusters caused by the Galactic tidal forces is slow so we expect a longer survival time for these clusters.

The tidal radius of clusters is influenced by the effects of Galactic tidal fields and internal relaxation dynamical evolution of clusters (Allen & Martos 1988). To find the tidal radius of Haffner 22 and Melotte 71, we have used the formula derived by Bertin & Varri (2008) as:

$$r_t = \left(\frac{GM_{cl}}{\omega^2 \nu}\right)^{1/3}$$

where ω and ν are

$$\omega = ((d\Phi_G(R)/dR)_{R_{gc}}/R_{gc})^{1/2}$$
$$\nu = 4 - \kappa^2/\omega^2$$

where κ is

$$\kappa = (3\omega^2 + (d^2\Phi_G(R)/dR^2)_{R_{gc}})^{1/2}$$

here Φ_G is Galactic potential, M_{cl} mass of the cluster, $R_{\rm gc}$ is the Galactocentric distance of the cluster, ω is the orbital frequency, κ is the epicyclic frequency and ν is a positive constant. We used above discussed Galactic potentials for this calculation, the value of the Galactocentric distance is taken from Table 9 and mass of the cluster is taken from Table 5. We

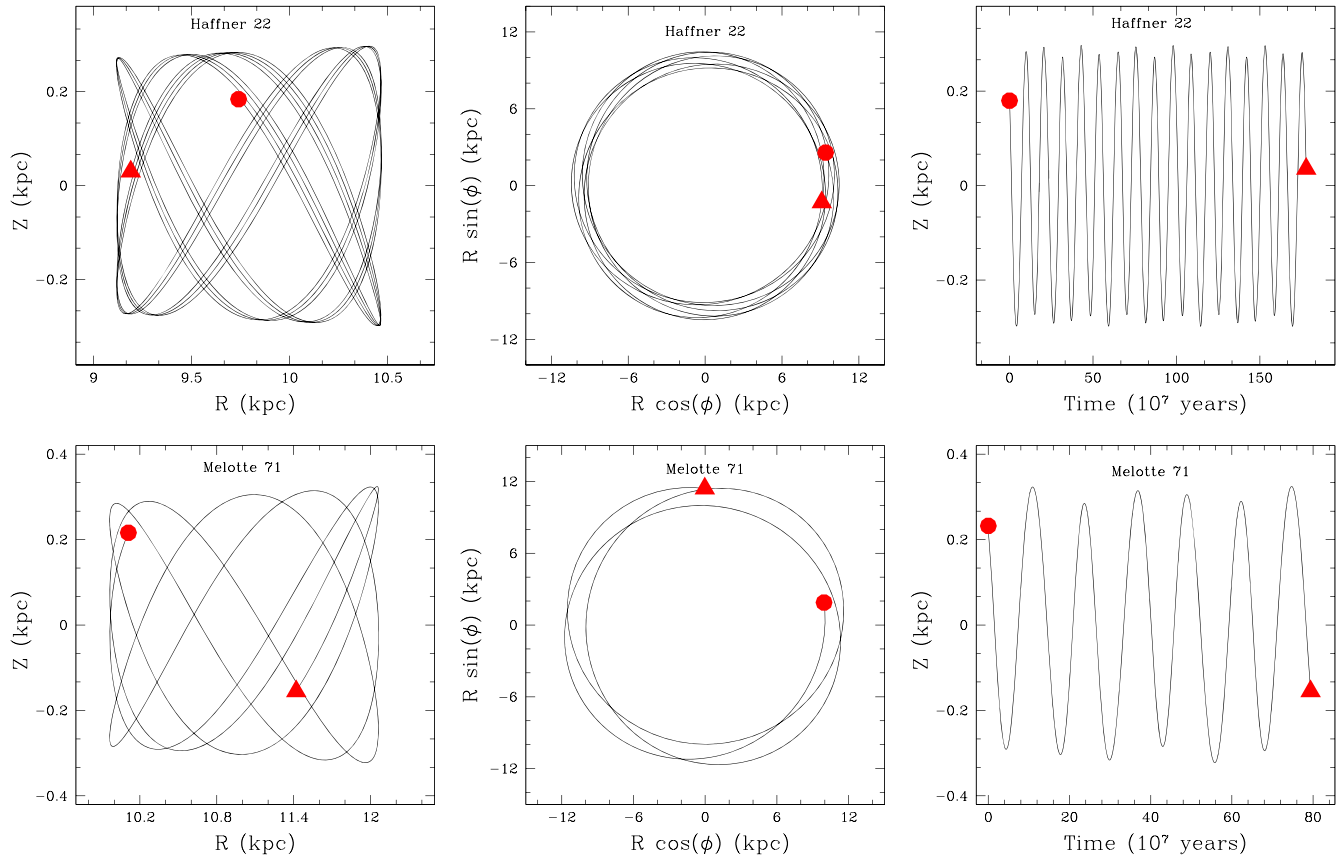

Figure 15. Galactic orbits of the clusters Haffner 22 and Melotte 71 estimated with the Galactic potential model described in text in the time interval of age of cluster. The left panels show the side view and the middle panels show the top view of the orbits. The right panels show the motion of both the clusters in the Galactic disk with time. The filled triangles and the circles denote the birth and the present day positions of the clusters in the Galaxy.

Table 7
Position and Velocity Components in the Galactocentric Coordinate System

Cluster	R (kpc)	Z (kpc)	U (km s^{-1})	V (km s^{-1})	W (km s^{-1})	ϕ (radian)
Haffner 22	9.75 ± 0.278	0.18 ± 0.029	23.29 ± 0.25	-245.75 ± 0.23	-12.17 ± 0.51	0.27
Melotte 71	10.11 ± 0.213	0.22 ± 0.016	-17.21 ± 0.35	-263.126 ± 0.32	-10.62 ± 0.36	0.19

Note. Here R is the galactocentric distance, Z is the vertical distance from the Galactic disk, U V W are the radial tangential and the vertical components of velocity respectively and ϕ is the position angle relative to the Sun's direction.

Table 8
Orbital Parameters Obtained Using the Galactic Potential Model

Cluster	e	R_a (kpc)	R_p (kpc)	$Z_{\max}$ (kpc)	E (100 km s^{-1})^2	J_z (100 kpc km s^{-1})	T_R (Myr)	T_Z (Myr)
Haffner 22	0.001	10.461	10.439	0.297	−9.988	−23.952	247	98
Melotte 71	0.004	11.584	11.491	0.324	−9.335	−26.610	240	102

Table 9
Various Fundamental Parameters of the Clusters Haffner 22 and Melotte 71

Parameter	Haffner 22	Melotte 71
R.A.	$123.^{\circ}1054 \pm 0.^{\circ}008$ ($8^{h}12^{m}25.^{s}2$)	$114.^{\circ}3854 \pm 0.^{\circ}004$ ($7^{h}37^{m}32.^{s}4$)
Decl.	$-27.^{\circ}9071 \pm 0.^{\circ}004$ ($-27^{\circ}54'25.''56$)	$-12.^{\circ}0598 \pm 0.^{\circ}003$ ($-12^{\circ}3'35.''28$)
Radius (arcmin)	5.5	6.5
Radius (parsec)	4.64	4.35
$\mu_{\alpha}\cos\delta$(mas yr^{-1})	-1.631 ± 0.009	-2.398 ± 0.004
μ_{δ}(mas yr^{-1})	2.889 ± 0.008	4.210 ± 0.005
Parallax (mas)	0.3547 ± 0.006	0.4436 ± 0.004
Age (Gyr)	2.25 ± 0.25	1.27 ± 0.14
Metal abundance	0.005	0.008
Distance modulus (mag)	12.80 ± 0.40	12.30 ± 0.30
Distance (Kpc)	2.88 ± 0.10	2.28 ± 0.15
X(Kpc)	-1.1042	-1.6395
Y(Kpc)	-2.5688	-1.8791
Z(Kpc)	0.1721	0.1995
R_{GC}(Kpc)	11.1491 ± 0.6	10.4627 ± 0.7
Total Luminosity (mag)	$\sim$2.5	$\sim$3.3
Cluster members	382	597
Relaxation time (Myr)	25	30
Dynamical evolution parameter (τ)	$\sim$90	$\sim$42

obtained tidal radius as 12.19 and 15.13 pc for the clusters Haffner 22 and Melotte 71, respectively.

7. Conclusions

We have analyzed two OCs, Haffner 22 and Melotte 71, based on the Gaia EDR3 photometric and astrometric database. We have recognized 382 and 597 likely members for the clusters Haffner 22 and Melotte 71, respectively, with membership probabilities higher than 50%. We studied the cluster structure, obtained the main fundamental parameters, described the dynamical study, and determined the galactic orbit of these clusters. The principal outcomes of this study can be summarized as follows:

1. The new center coordinates, cluster radius, and proper motions are obtained for Haffner 22 and Melotte 71 and are listed in Table 9. The enhancement of radius around $3.'5$ demonstrates the presence of a possible corona region for Haffner 22.
2. Our obtained distance values for both clusters from parallax are well supported by the values measured using the isochrone fitting approach to the CMDs. Ages of 2.25 ± 0.25 and 1.27 ± 0.14 Gyr were determined for the clusters Haffner 22 and Melotte 71, respectively. We have compared CMDs with the theoretical isochrones of metallicity $Z = 0.005$, 0.008 for Haffner 22 and Melotte 71, respectively, and as taken from Marigo et al. (2017).
3. We have detected five and four-member BSS in Haffner 22 and Melotte 71, respectively, and we found those identified BSS are confirmed members of the clusters.
4. Drawn on the relative number of high-velocity (binary) and single stars, we have determined the binary fractions for both clusters in the range of $\sim 10\% \leqslant f_{\rm bin} \leqslant 14\%$, for both core and o?-core regions. We obtained binary content is more in the core region for both clusters. Our investigation shows that proper motions turn out to be an essential tool for identifying high-velocity stars as unresolved binary cluster members.
5. The mass function slopes of 0.63 ± 0.30 and 1.23 ± 0.38 are obtained for the clusters Haffner 22 and Melotte 71, respectively. The MF slope for Melotte 71 is in good agreement within uncertainty with the value (1.35) given by Salpeter (1955). We found that a flat MF slope for Haffner 22 could hint at the mass segregation in this cluster. The total mass was estimated as 572 $M_{\odot}$ and 1015 $M_{\odot}$ for both clusters.
6. The evidence of mass segregation was observed for both clusters. The $(K-S)$ test indicates 88% and 80% confidence level for mass segregation in Haffner 22 and Melotte 71, respectively. Our estimated age values for both clusters are larger than their dynamic relaxation times, indicating that both clusters are dynamically relaxed.
7. The Galactic orbits and orbital parameters were evaluated for both clusters using Galactic potential models. We found Haffner 22 and Melotte 71 are orbiting in a boxy pattern outside the solar circle, and they trace the circular path around the center of the Galaxy. Both clusters are evolving slowly and are expected to survive for a longer lifetime.

The authors thank the anonymous referee for the useful comments that improved the scientific content of the article significantly. This work has been financially supported by the Natural Science Foundation of China (NSFC-11590782, NSFC-11421303). Devesh P. Sariya and Ing-Guey Jiang are supported by the grant from the Ministry of Science and Technology (MOST), Taiwan. The grant numbers are MOST 105-2119-M-007-029 -MY3 and MOST 106-2112-M-007-006 -MY3. This work has made use of data from the European Space Agency (ESA) mission Gaia (https://www.cosmos.esa.int/gaia), processed by the Gaia Data Processing and Analysis Consortium (DPAC, https://www.cosmos.esa.int/web/gaia/dpac/consortium). Funding for the DPAC has been provided by national institutions, particularly the institutions participating in the Gaia Multilateral Agreement. In addition to this, It is worth mentioning that this work has been done using WEBDA.

ORCID iDs

D. Bisht https://orcid.org/0000-0002-8988-8434
Qingfeng Zhu https://orcid.org/0000-0003-0694-8946
Devesh P. Sariya https://orcid.org/0000-0001-8452-7667
Ing-Guey Jiang https://orcid.org/0000-0001-7359-3300

References

Ahumada, J., & Lapasset, E. 1995, A&AS, 109, 375
Alcock, H., & Parker, R. J. 2019, MNRAS, 490, 350A
Allen, C., & Santillan, A. 1991, RMxAA, 22, 255
Allen, C., & Martos, M. 1988, RMxAA, 16, 25
Allison, R. J., Goodwin, S. P., Parker, R. J., et al. 2009, ApJ, 700, L99
Arenou, F., Luri,i, X., Babusiaux, C., et al. 2018, A&A, 616, A17
Auriere, M., Lauzeral, C., & Ortolani, S. 1990, Natur, 344, 638
Bailer-Jones, C. A. L. 2015, PASP, 127, 994
Bailer-Jones, C. A. L., Rybizki, J., Fouesneau, M., Mantelet, G., & Andrae, R. 2018, AJ, 156, 58
Bajkova, A. T., & Bobylev, V. V. 2016, AstL, 42, 9
Balaguer-Núñez, L., Tian, K. P., & Zhao, J. L. 1998, A&AS, 133, 387
Baumgardt, H., & Makino, J. 2003, MNRAS, 340, 227
Becker, W., & Fenkart, R. 1971, A&AS, 4, 241
Bellini, A., Piotto, G., Bedin, L. R., et al. 2009, A&A, 493, 959
Benz, W., & Hills, J. G. 1987, ApJ, 323, 614
Bertin, G., & Varri, A. L. 2008, ApJ, 689, 1005
Bica, E., & Bonatto, C. 2005, A&A, 431, 943
Bisht, D., Elsanhoury, W., Zhu, Q., et al. 2020a, AJ, 160, 119
Bisht, D., Zhu, Q., Elsanhoury, W., et al. 2021a, PASJ, 73, 677B
Bisht, D., Zhu, Q., Yadav, R. K. S., et al. 2020b, MNRAS, 482, 607
Bisht, D., Zhu, Q., Yadav, R. K. S., et al. 2021b, MNRAS, 503, 5929
Bobylev, V. V., Bajkova, A. T., & Gromov, A. O. 2017, AstL, 43, 4
Bonatto, C., & Bica, E. 2009, MNRAS, 397, 1915
Bossini, D., Vallenari, A., Bragaglia, A., et al. 2019, A&A, 623, A108
Bressan, A., Marigo, P., Girardi, L., et al. 2012, MNRAS, 427, 127
Brown, J. A., Wallerstein, G., Geisler, D., & Oke, J. B. 1996, AJ, 112, 1551B
Cantat-Gaudin, T., & Anders, F. 2020, A&A, 633, A99
Cantat-Gaudin, T., Jordi, C., Vallenari, A., et al. 2018, A&A, 618A, 93C
Cantat-Gaudin, T., Anders, F., Castro-Ginard, A., et al. 2020, A&A, 640, A1
Carraro, G., Selezine, A. F., Baume, G., & Turner, D. G. 2016, MNRAS, 455, 4031C
de La Fuente Marcos, R. 1996, A&A, 314, 453
Dias, W. S., Alessi, B. S., Moitinho, A., & Lepine, J. R. D. 2002, A&A, 389, 871
Dias, W. S., Monteiro, H., Caetano, T. C., et al. 2014, A&A, 564A, 79D
Dias, W. S., Monteiro, H., Lépine, J. R. D., et al. 2018, MNRAS, 481, 3887
Dib, S., & Henning, T. 2019, A&A, 629, 135
Dib, S., Kim, J., & Shadmehri, M. 2007, MNRAS, 381, L40
Dib, S., Schmeja, S., & Parker, R. J. 2018, MNRAS, 473, 849
Duquennoy, A., & Mayor, M. 1991, A&A, 248, 485
Eggen, O. J., & Iben, I. J. 1988, AJ, 96, 635
Eggen, O. J., & Iben, I. J. 1989, AJ, 97, 431
Ferreira, F. A., Corradi, W. J. B., Maia, F. F. S., Angelo, M. S., & Santos, J. F. C. J. 2020, MNRAS, 496, 2021
Fischer, P., Pryor, C., Murray, S., Mateo, M., & Richtler, T. 1998, AJ, 115, 592
Friel, E. D., & Janes, K. A. 1993, A&A, 267, 75
Gaia Collaboration, Brown, A. G. A., Vallenari, A., et al. 2021, A&A, 649, A1
Geller, A. M., & Mathieu, R. D. 2012, AJ, 144, 54
Girard, T. M., Grundy, W. M., Lopez, C. E., & van Altena, W. F. 1989, AJ, 98, 227
Goodwin, S. P., & Kroupa, P. 2005, A&A, 439, 565
Griffin, R. F., & Suchkov, A. A. 2003, ApJS, 147, 103
Hillenbrand, L. A., & Hartmann, L. W. 1998, ApJ, 492, 540
Johnson, H. L., & Sandage, A. R. 1955, ApJ, 121, 616
Kharchenko, N. V., Piskunov, A. E., Schilbach, S., Roeser, S., & Scholz, R. D. 2013, A&A, 558A, 53K
Kharchenko, N. V., Piskunov, A. E., Schilbach, S., Roeser, S., & Scholz, R. D. 2016, A&A, 585A, 101K
King, I. 1962, AJ, 67, 471
Kouwenhoven, M. B. N., Brown, A. G. A., Zinnecker, H., Kaper, L., & Portegies Zwart, S. F. 2005, A&A, 430, 137
Kroupa, P. 1995, MNRAS, 277, 1522
Kroupa, P. 1995a, MNRAS, 277, 1491
Kroupa, P. 1995b, MNRAS, 277, 1507
Kumar, B., Sagar, R., & Melnick, J. 2008, MNRAS, 386, 1380
Larsen, S. S. 2006, An ISHAPE Users Guide 14, arXiv:astro-ph/0701774
Lindegren, L., Bastian, U., Biermann, M., et al. 2021, A&A, 640, A1
Liu, L., & Pang, X. 2019, ApJS, 245, 32L
Lombardi, J. C., Rasio, F. A., & Shapiro, S. L. 1996, ApJ, 468, 797
Marigo, P., Bressan, A., Nanni, A., Girardi, L., & Pumo, M. L. 2013, MNRAS, 434, 488
Marigo, P., Girardi, L., Bressan, A., et al. 2017, ApJ, 835, 77
Mateo, M., Harris, H. C., Nemec, J., & Olszewski, E. W. 1990, AJ, 100, 469
Mathieu, R. D. 1984, ApJ, 284, 643
Mathieu, R. D. 1985, IAUS, 113, 427
Mathieu, R. D., & Latham, D. W. 1986, AJ, 92, 1364
McCrea, W. H. 1964, MNRAS, 128, 147
Mermilliod, J. C., Claria, J. J., Andersen, J., & Mayor, M. 1997, A&A, 324, 91M
Meylan, G. 2000, in ASP Conf. Ser. Massive Stellar Clusters, Conference Held in Strasbourg, France, ed. A. Lanon & C. Boily (San Francisco, CA: ASP), 215
Milone, A. P., Piotto, G., Bedin, L. R., et al. 2012, A&A, 540, A16
Monteiro, H., Dias, W. S., Moitinho, A., et al. 2020, MNRAS, 499, 1874
Nilakshi, S., & Sagar, R. 2002, A&A, 381, 65
Nilakshi, S., Sagar, R., Pandey, A. K., & Mohan, V. 2002, A&A, 383, 153
Pandey, A. K., Mahra, H. S., & Sagar, R. 1992, BASI, 20, 287
Pandey, A. K., Nilakshi, Ogura, K., Sagar, R., & Tarusawa, K. 2001, A&A, 374, 504
Pandey, A. K., Upadhyay, K., Ogura, K., et al. 2005, MNRAS, 358, 1290
Pavlik, V. 2020, A&A, 638, A155
Rain, M. J., Ahumada, J. A., & Carraro, G. 2021, A&A, 650A, 67R
Rangwal, G., Yadav, R. K. S., Durgapal, A., Bisht, D., & Nardiello, D. 2019, MNRAS, 490, 1383
Rastegaev, D. A. 2010, AJ, 140, 2013
Reid, M. J., & Brunthaler, A. 2004, ApJ, 616, 872
Romanishim, W., & Angel, J. R. P. 1980, ApJ, 235, 992
Salpeter, E. E. 1955, ApJ, 121, 161
Sampedro, L., Dias, W. S., Alfaro, E. J., Monteiro, H., & Molino, A. 2017, MNRAS, 470, 3937S
Sandage, A. R. 1962, ApJ, 135, 333
Sariya, D. P., Jiang, I.-G., Bisht, D., et al. 2021a, AJ, 161, 102
Sariya, D. P., Jiang, I.-G., Sizova, M. D., et al. 2021b, AJ, 161, 101
Schonrich, R., Binney, J., & Dehnen, W. 2010, MNRAS, 403, 1829S
Shao, Z., & Zhao, J. 1996, AcASn, 37, 377
Sim, G., Lee, S. H., Ann, H. B., & Kim, S. 2019, JKAS, 52, 145
Sollima, A. 2008, MNRAS, 388, 307
Soubiran, C., Cantat-Gaudin, T., Romero-Gómez, M., et al. 2018, A&A, 619, A155
Spitzer, L., & Hart, M. H. 1971, ApJ, 164, 399
Stryker, L. L. 1993, PASP, 105, 1081
Twarog, B. A., Corder, S., & Anthony-Twarog, B. J. 2006, AJ, 132, 299T
Williams, I. P. 1964, AnAp, 27, 198
Yang, X., Mo, H. J., van den Bosch, F. C., et al. 2005, MNRAS, 356, 1293